Open Access

Journal of Energy and Power Technology

LIDSEN Publishing Inc.

Research Article

Analysis of Correlations for the Prediction of the Entrainment Fraction of Droplets in Gas-liquid Annular Flows

Mariana P. Koss [†], Luiz E. M. Lima [†, *]

Department of Mechanics, Federal University of Technology — Paraná, Ponta Grossa, PR 84017-220, Brazil; E-Mails: marianakoss@alunos.utfpr.edu.br; lelima@utfpr.edu.br

† These authors contributed equally to this work.

* **Correspondence:** Luiz E. M. Lima; E-Mail: lelima@utfpr.edu.br

Academic Editor: Faik Hamad

Special Issue: Multi-phase Flow with and without Heat Transfer

Journal of Energy and Power Technology
2022, volume 4, issue 2
doi:10.21926/jept.2202019

Received: February 14, 2022
Accepted: May 06, 2022
Published: May 24, 2022

Abstract

In gas-liquid flows, droplets that detach from the liquid film lining the internal walls of a pipe and merge with the gas flowing through the pipe follow an annular flow pattern. This work analyzes correlations for estimating the entrainment fraction of such droplets contained in the literature by comparing their predictions with experimental data also from the literature. The results of this comparative study demonstrate that the analyzed correlations do not accurately reproduce experimental conditions. This is due to the complexity of this flow phenomenon and its arduous mathematical modeling. The methods used in the development of each correlation also impose operational limitations, and this parameter is difficult to measure satisfactorily on either a laboratory or industrial scale.

Keywords

Two-phase flow; annular flow; droplets; entrainment; correlation

1. Introduction

Multiphase flow occurs when two or more phases or chemical substances flow simultaneously. Such flow is found in several industrial systems, such as boiler pipes, evaporators, distillation towers, turbines, and chemical reactors [1]. Despite its complexity, this flow type can often be considered to be simply two-phase or two-component flow [2]. Two-phase flow, such as gas-liquid, can follow various flow patterns that are usually divided into three main groups: dispersed, intermittent, and separated. Annular flow, the object of study in this work, and stratified flow, both belong to the latter group.

In annular flow, there is a gaseous core, with or without the presence of liquid droplets, a liquid film, which lines the internal walls of a pipe, and a well-defined interface that separates these two phases or regions [3]. In vertical flows, the liquid film is considered to have a homogeneous thickness. However, in inclined or horizontal flows, the thickness of the lower part of the film is higher due to the gravitational force [1].

Understanding the characteristics of any droplets present in the gaseous core due to annular flow is essential in several situations to determine the characteristics of the pipe installations and the nature of the mass and heat transfer between gas and liquid phases. For example, the efficiency of nuclear reactor emergency cooling systems depends on the fraction of droplets present in the core, as does the feasibility and production efficiency in the chemical and petroleum industries [3-5]. The formation of droplets is related to the existence of waves generated in the film. For example, film turbulence and the changes in the gas flow velocity create waves. These waves break up, forming droplets when growing toward the gas flow due to the effects of interfacial shear stress between the gas and the liquid film [6].

In recent years there have been several research studies on the entrainment of droplets. Through experiment, Paleev and Filippovich [7] observed the relationship between different characteristics of fluids (density, dynamic viscosity, and surface tension) and flow parameters such as flow rate, to obtain a correlation for the entrainment of droplets. They did not observe any relationship between entrainment and pipe diameter. However, their correlation is not valid for small values of the ratio between the film and liquid (total) flow rates. Ishii and Mishima [4] developed a correlation using the Reynolds and Weber numbers, with variations for the inlet region and the quasi-equilibrium region, depending on the pipe diameter and the gas flow rate. Azzopardi and Zaidi [8] developed a new technique for measuring drop concentration in annular gas-liquid flow based on the scattering of light by the drops and used this to determine the entrainment fraction. Sawant et al. [9] developed a correlation that used the Reynolds and Weber numbers at the yield point of the film. However, Sawant et al. [10] later improved this correlation, incorporating the modified Weber numbers of the gas and the liquid viscosity. Al-Sarkhi and Sarica [11] proposed a correlation for the entrainment fraction applicable to low and high pressures data based on the Weber number of the superficial gas velocity that contained only two constants. Dasgupta et al. [12] presented a new method for predicting the entrainment fraction at the onset of annular flow based on the accuracy of the criterion for the transition to annular flow and a simplified triangular relationship. Bhagwat and Ghajar [13] introduced a correction factor that improves the accuracy of the Cioncolini and Thome [14] correlation by taking into account the effect of pipe orientation on the liquid entrainment fraction at high system pressures. Lee et al. [15] proposed new correlations to predict the entrainment fraction in horizontal pipes at low flow

rates of liquid based on the Pan and Hanratty [16] correlation, replacing the maximum entrainment model in their original equation with one taken from the literature. New correlations appear regularly, but, to date, there has not been an in-depth analysis.

Industrial-scale gas-liquid annular flows do not match those of experiments performed in the laboratory due to operational conditions, pipe dimensions pressure, and several other factors. Thus, it is difficult to find a sufficiently reliable and embracing correlation to estimate the entrainment fraction of droplets present in gas-liquid annular flows [1]. This work aims to perform a comparative analysis between many of the correlations available in the literature to estimate the entrainment fraction of the droplets for gas-liquid flows in the annular flow pattern and experimental data also available in the literature.

2. Materials and Methods

In this section, we describe the gas-liquid flow model for annular flow and the phenomenon, correlations, and experimental data for entrainment of droplets, as well as the method of analysis of the correlations.

2.1 Flow Model

The modeling of gas-liquid annular flow for a vertical or inclined pipe makes several assumptions [3]: one-dimensional (1D), uniformly distributed, and ascending flow; no change of phase of the components; acceleration is ignored in the conservation of momentum calculation; the densities, dynamics viscosities, and surface tension are constant for the liquid and gas phases; the mass flow rates (or superficial velocities) of the gas and liquid have known values, and the droplets have the same velocity as the gas in the core. Figure 1 shows a representation of gas-liquid annular flow.

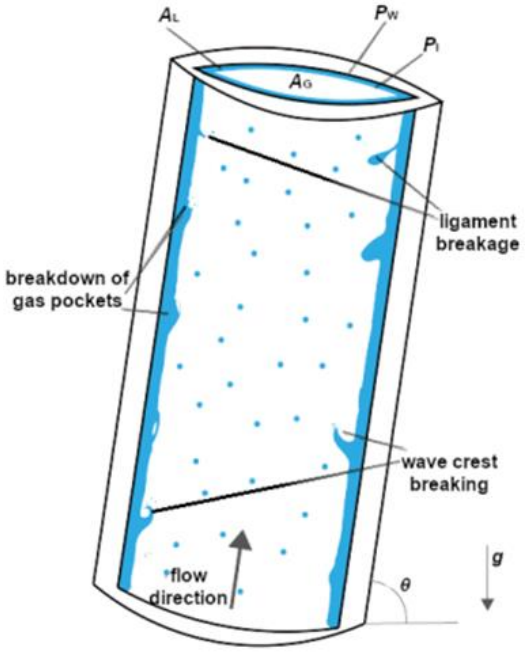

Figure 1 Diagram of gas-liquid annular flow.

The conservation of momentum for the core can be expressed as Equation (1):

$$-\frac{\mathrm{d}p}{\mathrm{d}z} = \rho_{\mathrm{C}} g \sin\theta + \frac{\tau_{\mathrm{I}} P_{\mathrm{I}}}{A_{\mathrm{G}}} \tag{1}$$

The conservation of momentum for the whole system can be expressed as Equation (2):

$$-\frac{\mathrm{d}p}{\mathrm{d}z} = \left(\frac{A_{\mathrm{G}}}{A}\rho_{\mathrm{C}} + \frac{A_{\mathrm{L}}}{A}\rho_{\mathrm{L}}\right) g \sin\theta + \frac{\tau_{\mathrm{W}} P_{\mathrm{W}}}{A} \tag{2}$$

Combining Equations (1) and (2) results in Equation (3), which can be used to determine the film thickness:

$$\frac{\tau_{\mathrm{W}} P_{\mathrm{W}}}{A} - \frac{\tau_{\mathrm{I}} P_{\mathrm{I}}}{A_{\mathrm{G}}} + \frac{A_{\mathrm{L}}}{A}(\rho_{\mathrm{L}} - \rho_{\mathrm{C}}) g \sin\theta = 0 \tag{3}$$

where p is the pressure, z is the axial coordinate, ρ is the density, g is the gravitational acceleration, θ is the pipe inclination, τ is the shear stress, P is the perimeter, and A is the cross-sectional area. The G, L, C, F, D, I, and W subscripts are gas, liquid, core, film, droplets, interface, and pipe wall identifiers, respectively.

The wall shear stress (τ_{W}) is defined as Equation (4):

$$\tau_{\mathrm{W}} = \frac{1}{2} f \rho_{\mathrm{L}} U_{\mathrm{L}}^2 \tag{4}$$

where $U_{\mathrm{L}} (\equiv J_{\mathrm{L}}/\alpha_{\mathrm{L}})$ is the actual velocity of the liquid, with the liquid superficial velocity being J_{L} and the liquid fraction (hold-up) being α_{L}; these definitions are analogous to those of a gas [17].

For the calculation of the turbulent Fanning friction factor (f), the Haaland equation [18] can be used (Equation (5)):

$$f = -3.6 \log\left[\left(\frac{\varepsilon/D}{3.7}\right)^{1.11} + \frac{6.9}{\mathrm{Re}}\right] \tag{5}$$

where ε and D are the absolute roughness and diameter of the pipe, respectively, and the Reynolds number is expressed by $\mathrm{Re} = JD\rho/\mu$, with μ being the dynamic viscosity.

Interfacial shear stress (τ_{I}) occurs due to differences in the properties and velocities of the core and the film. It can be written as Equation (6) [5, 19]:

$$\tau_{\mathrm{I}} = \frac{1}{2} f_{\mathrm{I}} \rho_{\mathrm{C}} (U_{\mathrm{G}} - U_{\mathrm{L}})^2 \tag{6}$$

Several correlations available in the literature, such as that of Pedras [5], calculate the interfacial friction factor (f_{I}) as according to Equation (7):

$$f_{\mathrm{I}} = 7.8 \times 10^{-3} + 52\left(\frac{\rho_{\mathrm{G}}}{\rho_{\mathrm{L}}}\right)\left(1 - \sqrt{\alpha_{\mathrm{G}}}\right)\mathrm{Re}_{J_{\mathrm{G}},J}^{2/5} \tag{7}$$

where α_{G} is the gas fraction (Equation (8)), and $\mathrm{Re}_{J_{\mathrm{G},J}}$ is a gas Reynolds number calculated from the average drift velocity of the gas ($J_{\mathrm{G},J}$) (Equation (9)):

$$\frac{\alpha_{\mathrm{G}}}{1-\alpha_{\mathrm{G}}} = 1.255 \times 10^{-3} \mathrm{Re}_{\mathrm{L}}^{0.56} \left| \frac{J_{\mathrm{G}}}{J_{\mathrm{L}}} \right| \tag{8}$$

$$J_{\mathrm{G},J} = \left(\frac{1}{1.255 \times 10^{-3} \mathrm{Re}_{\mathrm{L}}^{0.56}} - 1 \right) J_{\mathrm{L}} \tag{9}$$

The core density (ρ_{C}) is defined by Equation (10):

$$\rho_{\mathrm{C}} = \frac{\dot{m}_{\mathrm{G}} + \dot{m}_{\mathrm{D}}}{\frac{\dot{m}_{\mathrm{G}}}{\rho_{\mathrm{G}}} + \frac{\dot{m}_{\mathrm{D}}}{\rho_{\mathrm{L}}}} \tag{10}$$

where the mass flow rate is $\dot{m}$. As in several other models available in the literature, the determination of the mass flow rate of droplets ($\dot{m}_{\mathrm{D}}$) is obtained here from knowledge of the entrainment fraction of droplets, frequently predicted using empirical correlations.

2.2 Entrainment Phenomenon

According to Ishii and Mishima [4], there are two ways to measure the entrainment fraction of droplets within gas-liquid annular flows. The first is with a probe placed in the center of the pipe and assuming the distribution of droplets to be uniform. This method has flaws when there is a high flow rate of liquid since there is a possibility that the probe also measures the film because of turbulence on the film surface. A second, more rigorous approach is to remove the liquid film through a porous wall in the pipe immediately before the test section, with the liquid being routed back through the cyclone to return to the experiment [20]. The fraction of droplets that remain in the gaseous medium can be measured using one of several techniques, such as diffraction methods [21], photography and sedimentation [22], or a conductivity probe [23]. The test section inlet geometry has a significant influence, requiring that measurements be conducted some distance from the inlet for the correct results to be obtained [4].

The entrainment of droplets from the film to the gas core depends on both the gas velocity and the liquid mass flow rate. Figure 1 illustrates the three most common types of entrainment of droplets [24, 25]: 1) wave crest breaking, where an agitation wave grows toward the core and breaks up into droplets; 2) the breakdown of gas pockets present in the film due to the high surface tension; and 3) ligament breakage, where the difference in superficial velocities of the gas and liquid, leads to the formation of a ligament and its breakage.

Using an experiment employing water and gas, Zhang et al. [26] used Laser Doppler Anemometry (LDA) to observe the influence of relevant variables on the entrainment of droplets in annular and churn flow environments, as shown in Figure 2.

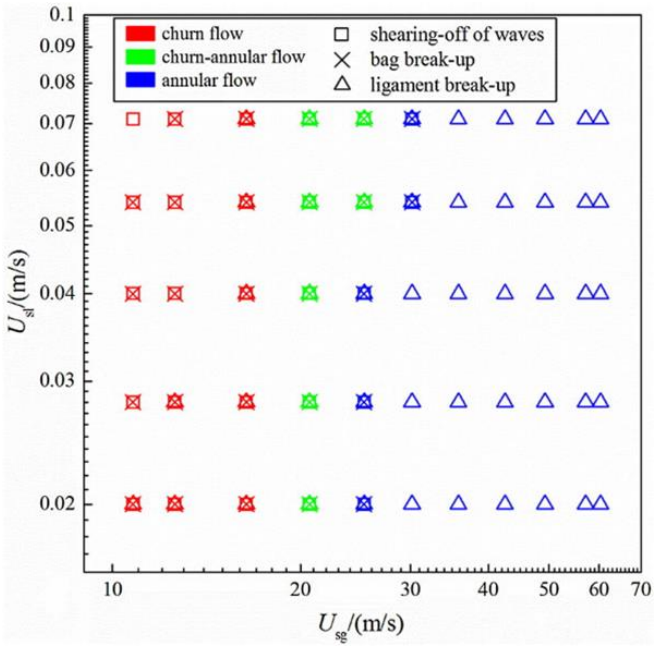

Figure 2 Types of entrainments of droplets divided according to liquid and gas superficial velocities [26].

2.3 Empirical Correlations

Given the complexity of the theoretical modeling of the phenomenon, all of the existing correlations that have been developed for the entrainment fraction of droplets (E) have used an empirical approach. Table 1 lists the correlations used in this work, the details of which are given in the rest of this section.

Table 1 Correlations for the entrainment fraction of droplets analyzed in this work.

Author(s)	Correlation
Paleev and Filippovich [7]	$E = 0.015 - 0.44 \log\left[10^4 \frac{\rho_C}{\rho_L}\left(\frac{J_G \mu_C}{\sigma}\right)\right]$
Owen [25]	$\frac{E}{E_{max}} = \begin{cases} \exp(-6.8872 + 0.472 \ln I_m) & \text{if } I_m < 1.35 \times 10^6 \\ 0.69 + 8.03 \times 10^{-8} I_m & \text{if } 1.35 \times 10^6 \le I_m \le 2.15 \times 10^6 \\ \exp(-1.775 + 0.112 \ln I_m) & \text{if } I_m > 2.15 \times 10^6 \end{cases}$
Oliemans et al. [3]	$\frac{E}{1-E} = 10^{\beta_0} \rho_L^{\beta_1} \rho_G^{\beta_2} \mu_L^{\beta_3} \mu_G^{\beta_4} \sigma^{\beta_5} D^{\beta_6} J_L^{\beta_7} J_G^{\beta_8} g^{\beta_9}$
Ishii and Mishima [4]	$E = \tanh\left(7.25 \times 10^{-7} \mathrm{Re}_L^{1/4} \mathrm{We}_{G,mod}^{5/4}\right)$
Pan and Hanratty [16]	$\frac{E/E_{max}}{1-E/E_{max}} = 9 \times 10^{-9} \left(\frac{J_G^3 D \sqrt{\rho_G \rho_L}}{\sigma}\right) \sqrt{\frac{\rho_G^{1-m} \mu_G^m}{g d_{32}^{1+m} \rho_L}}$
Pan and Hanratty [27]	$\frac{E/E_{max}}{1-E/E_{max}} = 8.8 \times 10^{-5} \left(\frac{J_G^3 D \sqrt{\rho_G \rho_L}}{\sigma}\right)$

Sawant et al. [9]	$\frac{E}{E_{\max}} = \tanh\left(2.13 \times 10^{-4} \mathrm{Re}_{\mathrm{L}}^{-0.35} \mathrm{We}_{\mathrm{G,mod}}^{5/4}\right)$
Sawant et al. [10]	$\frac{E}{E_{\max}} = \tanh\left[2.13 \times 10^{-4} \mathrm{Re}_{\mathrm{L}}^{-0.35} \left(\mathrm{We}_{\mathrm{G,mod}} - \mathrm{We}_{\mathrm{G,crit}}\right)^{5/4}\right]$
Karami et al. [28]	$\frac{E/E_{\max}}{1-E/E_{\max}} = 3 \times 10^{-8} \mathrm{We}_{\mathrm{G,mod}}^{5/4} \left(\frac{J_{\mathrm{G}} - J_{\mathrm{G,atom}}}{J_{\mathrm{G,crit}}}\right) \frac{D}{S_{\mathrm{atom}}} \sqrt{\frac{\rho_{\mathrm{L}}}{\rho_{\mathrm{G}}}}$

Paleev and Filippovich [7] used a horizontal pipeline to develop a correlation for the entrainment fraction of droplets across a range of a ratio of 0.02 kg to 0.12 kg of water for every 1 kg of air and $3 \times 10^4 \leq \mathrm{Re}_{\mathrm{G}} \leq 8.5 \times 10^4$. The data used in their work were from both vertical and horizontal pipes, which explains the dispersion seen in the results. They found no relationship between the pipe diameter and entrainment fraction of droplets. However, their correlation is not recommended for small values of the ratio between the film and liquid (total) mass flows ($\dot{m}_{\mathrm{F}}/\dot{m}_{\mathrm{L}}$). The expression they used for the core density (ρ_{C}) was Equation (11):

$$\rho_{\mathrm{C}} = \rho_{\mathrm{G}} \left(1 + E \frac{J_{\mathrm{L}}}{J_{\mathrm{G}}} \frac{\rho_{\mathrm{L}}}{\rho_{\mathrm{G}}}\right) \tag{11}$$

Owen [25] developed correlations for vertical pipes, 32-mm in diameter with air-water flows, and pre-determined pressures and variation in gas and liquid velocities. He used the models of Ishii and Mishima [29], considering the interpolation ranges of the dimensionless group (I_m) as shown in Equations (12) and (13). He observed a maximum point on the pressure gradient curve as a function of gas flow rate, which was identical to the pressure gradient found in the hydraulic resistance crisis phenomenon [30]. The dimensionless group I_m is given by Equation (12):

$$I_m = (J_{\mathrm{G}}^*)^{5/2} (D^*)^{3/2} \, \mathrm{Re}_{\mathrm{L}}^{1/4} \tag{12}$$

The dimensionless gas superficial velocity (J_{G}^*) is calculated by Equation (13) [25]:

$$J_{\mathrm{G}}^* = \frac{J_{\mathrm{G}}}{\left[\frac{g\sigma\Delta\rho}{\rho_{\mathrm{G}}^2} \left(\frac{\rho_{\mathrm{G}}}{\Delta\rho}\right)^{2/3}\right]^{1/4}} \tag{13}$$

The dimensionless hydraulic diameter is given by $D^* = \sqrt{\mathrm{Eo}}$, with the Eötvös number being given by $\mathrm{Eo} = gD^2\Delta\rho/\sigma$, where σ is the gas-liquid surface tension. The maximum entrainment ($E_{\max}$) is the upper limiting value of this parameter, and for which a liquid film must exist at the bottom of a horizontal pipe, begin defined by Equation (14) [25]:

$$E_{\max} = \frac{1 - \mathrm{Re}_{\mathrm{L,crit}}}{\mathrm{Re}_{\mathrm{L}}} \tag{14}$$

The critical liquid Reynolds number ($\mathrm{Re}_{\mathrm{L,crit}}$) is given by Equation (15) [25]:

$$\mathrm{Re}_{\mathrm{L,crit}} = \exp\left[5.8405 + 0.4249 \left(\frac{\mu_{\mathrm{G}}}{\mu_{\mathrm{L}}}\right) \sqrt{\frac{\rho_{\mathrm{L}}}{\rho_{\mathrm{G}}}}\right] \tag{15}$$

Oliemans et al. [3] used data from the Harwell database [31] to model the correlations between the interfacial friction factor and the entrainment fraction of droplets. The diameters of the pipes that they studied varied from 9 mm to 20 mm, and the flow was turbulent. They closed their correlation using the adjustment coefficients shown in Table 2. However, the parameters used indicated that entrainment of droplets increased with increasing pipe diameter due to the β_6 value (adjustment coefficient for diameter), contradicting the results of other studies, such as that of Ishii and Mishima [4].

Table 2 Values for the adjustment coefficients of the correlation of Oliemans et al. [3].

β_0	β_1	β_2	β_3	β_4	β_5	β_6	β_7	β_8	β_9
-2.52	1.08	0.18	0.27	0.28	-1.80	1.72	0.70	1.44	0.46

Ishii and Mishima [4] developed a correlation using dimensionless parameters for flows in vertical pipes based on the wave-crest-breaking entrainment mechanism. They also considered the effect of the length of the flow inlet region (z_{in}), defined in Equation (16), and introduced a modified Weber number of the gas ($\mathrm{We}_{\mathrm{G,mod}}$), defined in Equation (17). The correlation showed satisfactory results for pipe diameters from 9.5 mm to 32 mm, pressures from 1 atm to 4 atm, Reynolds number from 370 to 6400, and core velocities lower than 100 m/s.

$$z_{\mathrm{in}} \geq 600D\sqrt{\frac{J_{\mathrm{G}}^{*}}{\mathrm{Re}_{\mathrm{L}}}} \tag{16}$$

$$\mathrm{We}_{\mathrm{G,mod}} = \frac{J_{\mathrm{G}}^{2} D \rho_{\mathrm{G}}}{\sigma}\left(\frac{\Delta\rho}{\rho_{\mathrm{G}}}\right)^{1/3} \tag{17}$$

Pan and Hanratty [16, 27] used experiment and theory to develop correlations for both horizontal [16] and vertical [27] pipes using air and water as fluids. The gas velocities were low in the horizontal pipes and high in the vertical pipes. The pipe diameter in their studies ranged from 9.53 mm to 23.1 mm, the mass flow rate of the liquid varied from 0.003 kg/s to 0.97 kg/s, and the gas velocity ranged from 11 m/s to 131 m/s. The exponent m was defined as zero when within the Newton regime, one when within the Stokes regime, and 0.6 when $1.92 \leq \mathrm{Re} \leq 500$. In this work, we use $m = 0.6$. The critical liquid Reynolds number ($\mathrm{Re}_{\mathrm{L,crit}}$) is defined as Equation (18):

$$\mathrm{Re}_{\mathrm{L,crit}} = 7.3(\log\omega)^3 + 44.2(\log\omega)^2 - 263\log\omega + 439 \tag{18}$$

where the dimensionless parameter ω is $= (\mu_{\mathrm{L}}/\mu_{\mathrm{G}})\sqrt{\rho_{\mathrm{L}}/\rho_{\mathrm{G}}}$.

Sawant et al. [9] developed a correlation employing two dimensionless numbers (Reynolds and Weber) to estimate the entrainment fraction of droplets in air-water flows. This correlation was considered to work well for the gas velocity values they used in the experiments at high pressure. However, they indicated the need to use a better correlation to estimate the maximum entrainment fraction of droplets. In their tests, the diameter of the pipes was 9.4 mm, the pressure varied from 1.2 bar to 6 bar, the superficial velocity of the liquid varied from 0.05 m/s to 0.5 m/s, and the superficial gas velocity varied from 15 m/s to 100 m/s, with both velocities varying according to the pressure used. They expressed the maximum entrainment fraction of

droplets analogously to Equation (14) but using a minimum film Reynolds number ($\mathrm{Re}_{\mathrm{F,min}}$), defined by Equation (19), in place of the critical liquid Reynolds number ($\mathrm{Re}_{\mathrm{L,crit}}$):

$$\mathrm{Re}_{\mathrm{F,min}} = 250 \ln \mathrm{Re}_{\mathrm{L}} - 1265 \tag{19}$$

Sawant et al. [9] also considered a modified gas Weber number ($\mathrm{We}_{\mathrm{G,mod}}$) given by Equation (20):

$$\mathrm{We}_{\mathrm{G,mod}} = \frac{J_{\mathrm{G}}^2 D \rho_{\mathrm{G}}}{\sigma} \left(\frac{\Delta\rho}{\rho_{\mathrm{G}}}\right)^{1/4} \tag{20}$$

Sawant et al. [10] used additional experimental datasets to describe the phenomenon and establish a new correlation adapted from the one developed by Sawant et al. [9]. The fluids used were air and water and an organic fluid (Freon-113) that exists as a vapor-liquid mixture at high pressure. The pressure ranged from 1.2 bar to 6.0 bar in a 9.4 mm diameter pipe, for the air-water experiment, and from 2.8 bar to 8.5 bar in a 10.2 mm diameter pipe, for the organic fluid. However, the correlation proved not to be able to reproduce data in the literature, probably due to the film extraction method used. In this modified correlation, the minimum film Reynolds number ($\mathrm{Re}_{\mathrm{F,min}}$) is defined using Equation (21):

$$\mathrm{Re}_{\mathrm{F,min}} = 13 N_{\mu_{\mathrm{L}}}^{-1/2} + 0.3\left(\mathrm{Re}_{\mathrm{L}} - 13 N_{\mu_{\mathrm{L}}}^{-1/2}\right)^{0.95} \tag{21}$$

where the liquid viscosity number, $N_{\mu_{\mathrm{L}}}$, is given by Equation (22) [10]:

$$N_{\mu_{\mathrm{L}}} = \frac{\mu_{\mathrm{L}}}{\left(\frac{\sigma^3 \rho_{\mathrm{L}}^2}{g\Delta\rho}\right)^{1/4}} \tag{22}$$

and the critical gas Weber number, $\mathrm{We}_{\mathrm{G,crit}}$, is given by Equation (23) [10]:

$$\mathrm{We}_{\mathrm{G,crit}} = \frac{J_{\mathrm{G,crit}}^2 D \rho_{\mathrm{G}}}{\sigma} \left(\frac{\Delta\rho}{\rho_{\mathrm{G}}}\right)^{1/4} \tag{23}$$

Karami et al. [28] performed experiments with multiphase flows in a 152-mm diameter horizontal pipe, using air, Isopar L oil, and water as the fluids. The pressure during the experiments remained constant, despite the variations in the flow rates of the fluids. The atomization length of the droplets (S_{atom}) is defined by Equation (24), the atomization superficial gas velocity ($J_{\mathrm{G,atom}}$) is based on the wave transition relationship described by Andritsos and Hanratty [32] (Equation (25)), and for the critical gas superficial velocity ($J_{\mathrm{G,crit}}$) the Pan and Hanratty correlation [16] is used, (Equation (26)). The latter is also used for the maximum entrainment (E_{max}):

$$S_{\mathrm{atom}} = P\left[0.62\alpha_{\mathrm{L}}^{0.374}\left(\frac{0.07}{\sigma}\right)^{0.15} + \frac{\mathrm{Fr}_{\mathrm{G}}^{4/5}\mathrm{We}_{\mathrm{G}}^{1/4}}{\cos\theta}\left(\frac{\rho_{\mathrm{G}}}{\Delta\rho}\right)\right] \tag{24}$$

$$J_{\mathrm{G,atom}} = 5\sqrt{\frac{\rho_{\mathrm{G,0}}}{\rho_{\mathrm{G}}}} \tag{25}$$

$$J_{\mathrm{G,crit}} = \frac{gD^{1.6}\Delta\rho}{13.9\rho_{\mathrm{G}}^{2/5}\mu_{\mathrm{G}}^{3/5}} \tag{26}$$

where the liquid fraction (hold-up) is $\alpha_{\mathrm{L}} = 1 - \alpha_{\mathrm{G}}$, the gas Froude number is $\mathrm{Fr}_{\mathrm{G}} = J_{\mathrm{G}}/\sqrt{gD}$, and the gas Weber number is $\mathrm{We}_{\mathrm{G}} = J_{\mathrm{G}}^2 D\rho_{\mathrm{G}}/\sigma$.

2.4 Experimental Data

Researchers have used a variety of different methods of experimental determination to obtain empirical data on the phenomenon of the entrainment fraction of droplets. We use experimental data obtained by MacGillivray [33] and Kesana et al. [34] in our comparative study of correlations of entrainment fraction of droplets contained in the literature.

MacGillivray [33] performed experiments onboard the Novespace Airbus 310 Zero-G airplane (https://www.airzerog.com/) under micro, hyper, and normal gravity to analyze the effect of gas density and gravitational acceleration on film thickness and frictional pressure loss in annular helium-water and air-water flows. We use the results obtained for air-water in normal gravity as the correlations described in the previous section are often applicable in this case.

Under low film flow conditions, Kesana et al. [34] analyzed the effects of the system pressure, gas and liquid flow rates, and the piping material on the entrainment of droplets, using Sulfur Hexafluoride (SF_6) with a high density as the gas phase, and Exxsol D60 oil as the liquid phase. The pipes used were made of polyvinyl chloride (PVC) and carbon steel.

Table 3 lists the key pipe and fluid characteristics for the experimental datasets of MacGillivray [33] and Kesana et al. [34].

Table 3 Key characteristics of the experimental datasets used in this work.

Parameter	**MacGillivray [33]**	**Kesana et al. [34]**	
		PVC	**Carbon steel**
D/(mm)	9.525	100	100
ε/(μm)	1.5	2	40
ρ_{L}/(kg/m^3)	998	810	810
μ_{L}/(MPa/s)	1.01	1.41	1.41
μ_{G}/(MPa/s)	0.0181	0.015	0.015
σ/(mN/m)	72.7	28.5	28.5

2.5 Analytical Method

For the analysis of the performance of the correlations with the experimental data, a program was written using Python™ [35]. Python is an expressive programming language with a simple and efficient object-oriented syntax that is ideal for handling databases [36]. The following Python libraries were used:

- Pandas [37] - used to import, process, and build the data tables (read and write Excel sheets using the DataFrame feature, construct Series and a DataFrame, and configure and customize the DataFrame).

- Numpy [38] - used for math operations, with features such as extended precision (float64), conditional (where), non-negative square root (sqrt), exponential (exp), natural logarithm (log), base-10 logarithm (log10), cosine (cos), hyperbolic tangent (tanh), and pi.
- Scikit-learn (sklearn.metrics) [39] - used for calculating the errors between theoretical results and experimental data (mean square error, mean absolute error, and mean absolute percentage deviation).

The Plotly graphing package [40] was also used to produce the graphs employed in the analysis of the results. After importing the data using Pandas, the correlations and auxiliary equations (shown in Section 2.3) were written using functions. Each of these functions is called within a loop using the imported data tables to allow the execution of the necessary calculations. Each computed entrainment fraction of droplets (E) had its values adjusted such that $0 \leq E \leq 1$. Valid results were saved to another table and classified by the correlation used. These data were then plotted to find trends in correlation behavior and to verify the accuracy of the results. Finally, the code calculated deviations (standard, mean squared, absolute, and relative) and variances. The results of this exercise are presented and discussed in the next section.

3. Results and Discussion

The results of the analysis were separated into three cases according to the experimental data used: Case 1, with data from MacGillivray [33], and Cases 2 and 3, with data from Kesana et al. [34] for PVC and carbon steel pipes, respectively. For each case, the influence of the superficial velocity of the gas was analyzed using the data of the calculated entrainment fraction of droplets (E) as a function of the gas Reynolds number ($\mathrm{Re_G}$), all other parameters in the Reynolds number calculation being considered equal, and comparisons were made between the results of the correlations and the experimental values to determine the degree of deviation between the two.

3.1 Case 1

As Figure 3(a) shows, E is directly proportional to $\mathrm{Re_G}$. This is due to the increase in core turbulence with higher $\mathrm{Re_G}$ values, influencing the interfacial friction factor and the interfacial shear stress (Equations (8) and (7), respectively). This increase in core turbulence causes the waves on the film's surface to break and subsume the droplets released into the core. To observe the precision of the E values calculated using the correlations, Figure 3(b) shows the theoretical-experimental comparison, with the diagonal line representing the case of zero-deviation between the values. As can be seen, in the experimental data E varies from 0.8 to 1.0. MacGillivray [33] used a conductive wire probe to measure the film thickness, which may have resulted in an overestimation of the E values in comparison to the values calculated by the correlations analyzed in this work, along with other factors.

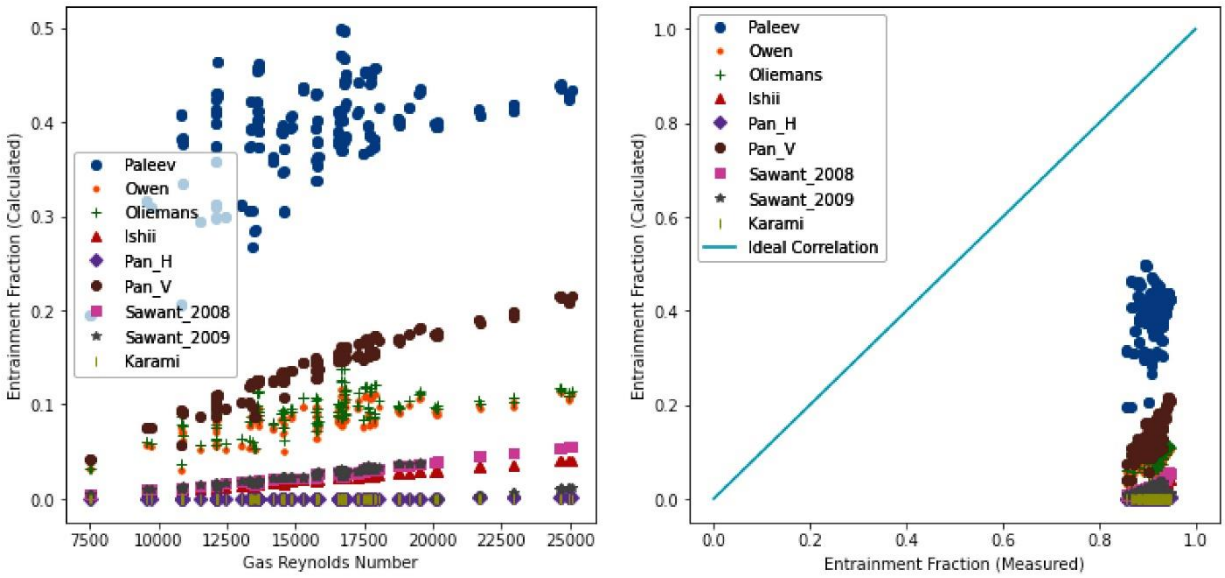

Figure 3 Case 1: (a) E as a function of $\mathrm{Re_G}$ and (b) the theoretical-experimental comparison.

The correlation results of Paleev and Filippovich [7] are considerably higher than those of the other correlations. This correlation overestimates the entrainment of droplets and does not consider the pipe diameter effect, as observed by Kesana et al. [34]. The correlations by Oliemans et al. [3], Owen [25], and Pan and Hanratty [27] present similar results to each other as they used identical considerations and approaches. The two correlations by Sawant et al. [9, 10] use a modified gas Weber number that is different from that used by Ishii and Mishima [4], but the results show some similarity. The E values calculated using the correlation of Sawant et al. [10] are very low, approaching zero for lower $\mathrm{Re_G}$ values.

Table 4 shows the values of standard deviation (σ_E), variance (σ_E^2), mean squared deviation (ϵ_1), absolute deviation (ϵ_2), and relative deviation (ϵ_3) for each correlation. The divergence between the experimental data and the calculated values is obvious, with instances of absolute deviations of 100%.

Table 4 Deviations between experimental results and the correlations under study for Case 1.

Correlation	σ_E	σ_E^2	ϵ_1	ϵ_2	ϵ_3/(%)
Paleev and Filippovich [7]	0.052292	0.002734	0.272940	0.519828	56.99
Owen [25]	0.017715	0.000314	0.684499	0.827095	90.68
Oliemans et al. [3]	0.019439	0.000378	0.672113	0.819503	89.85
Ishii and Mishima [4]	0.007752	0.000060	0.795881	0.892010	97.80
Pan and Hanratty [16]	0.000371	0.000000	0.831660	0.911747	99.95
Pan and Hanratty [27]	0.034217	0.001171	0.596839	0.772232	84.71
Sawant et al. [9]	0.010884	0.000118	0.786202	0.886602	97.22
Sawant et al. [10]	0.009105	0.000083	0.793558	0.890615	97.64
Karami et al. [28]	0.000000	0.000000	0.832393	0.912143	100.00

3.2 Case 2

Figures 4(a) and 4(b) show the E versus $\mathrm{Re_G}$ and theoretical-experimental comparison graphs, respectively, for Case 2, and Table 5 shows the deviations. The calculated values with the correlation of Paleev and Filippovich [7] did not converge using the data from Kesana et al. [34], possibly because of the divergence between the key characteristics of the pipes and fluids of these two studies. In the experiment carried out by Kesana et al. [34], 26 tests were performed at different gas and liquid velocities and gas density/pressure, parameters that directly influence $\mathrm{Re_G}$, as seen in Figure 4(a), where there are several points with the same $\mathrm{Re_G}$ value, but different E values. This implies that $\mathrm{Re_G}$ is not the only factor influencing the value of E. As Figure 4(b) shows, for high values of E, the results of the correlations by Oliemans et al. [3], Ishii and Mishima [4], and Sawant et al. [10] are the closest to the experimental results, despite the low precision. Most of the calculated results overestimate E, as can be seen in the concentration of points on the left side of the diagonal line of the graph. There are even instances of complete overestimation ($E = 1$), and underestimation ($E = 0$).

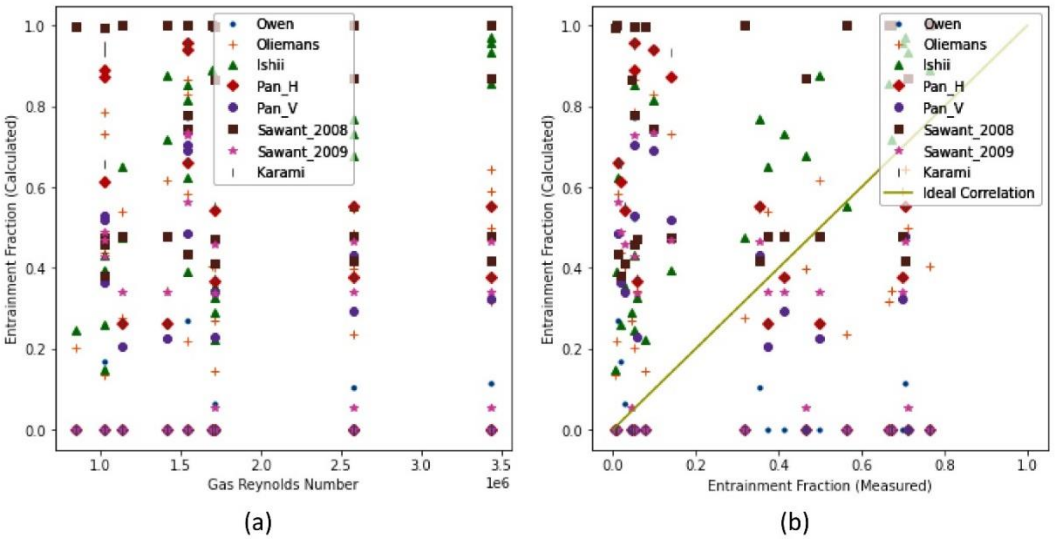

Figure 4 Case 2: (a) E as a function of $\mathrm{Re_G}$ and (b) theoretical-experimental comparison.

Table 5 Deviations between the experimental results and the correlations under study for Case 2.

Correlation	σ_E	σ_E^2	ϵ_1	ϵ_2	ϵ_3/(%)
Owen [25]	0.233755	0.054641	0.209693	0.379037	320.73
Oliemans et al. [3]	0.209538	0.043906	0.137427	0.296748	726.66
Ishii and Mishima [4]	0.263295	0.069324	0.117955	0.291718	742.44
Pan and Hanratty [16]	0.348001	0.121104	0.260907	0.415625	682.09
Pan and Hanratty [27]	0.241589	0.058365	0.176067	0.346567	466.16
Sawant et al. [9]	0.258461	0.066802	0.288907	0.450687	1631.25
Sawant et al. [10]	0.249134	0.062068	0.178722	0.343815	530.89
Karami et al. [28]	0.358599	0.128594	0.271757	0.422940	700.92

Table 5 shows the deviations of correlations compared to data from Kesana et al. [34] for Case 2 (PVC piping). The standard deviations of the correlations are higher than in the case of the data by MacGillivray [33], showing that the calculated values of E are more dispersed. The absolute deviation values are also significantly higher. Kesana et al. [34] used SF_6 and Exxsol D60 as gas and liquid, respectively, while most of the correlations analyzed in this work used air and water in the experiments that formed the basis for their development. Furthermore, Kesana et al. [34] used a horizontal pipe, while the only correlations based on experiments with horizontal pipes analyzed in this work are those of Pan and Hanratty [16] and Karami et al. [28], which may also explain the divergence of results.

3.3 Case 3

In the experiments by Kesana et al. [34] with a carbon steel pipe, eight tests were performed at only gas superficial velocities (7.5 m/s and 10.0 m/s), resulting in a concentration of the points in the only two $\mathrm{Re_G}$ values obtained, as shown in Figure 5(a). In Figure 5(b), there are clusters of points to the left and the right of the diagonal line, representing the overestimation and underestimation of E values, respectively.

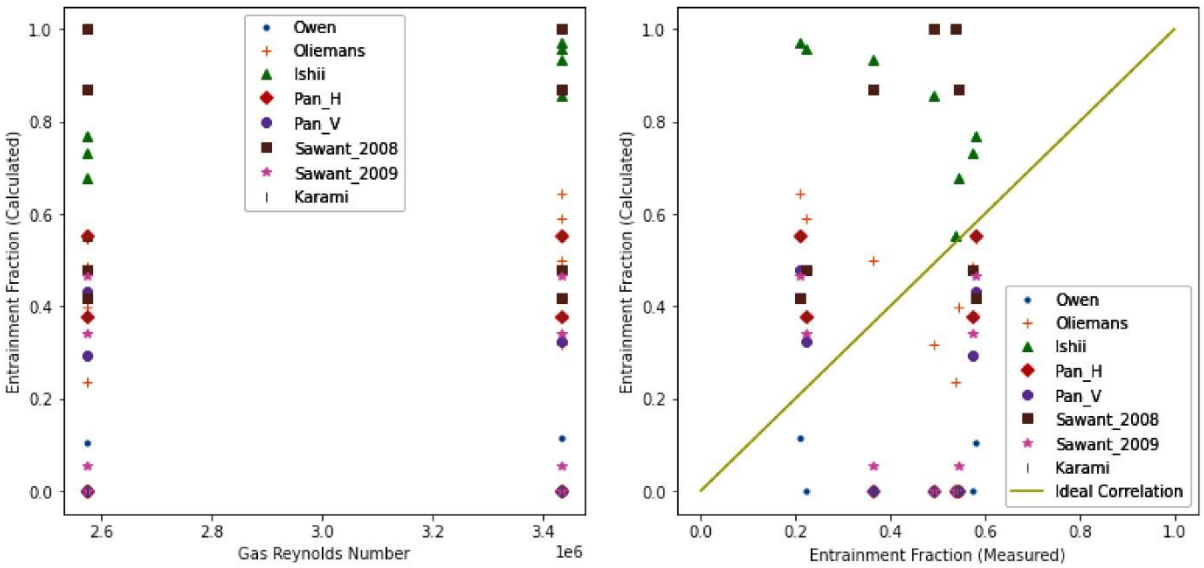

Figure 5 Case 3: (a) E as a function of $\mathrm{Re_G}$ and (b) theoretical-experimental comparison.

As with the other two cases, no correlation precisely agrees with the experimental values. In addition, Kesana et al. [34] observed that the E values found with PVC piping are higher than those found with carbon steel piping due to differences in the absolute roughness of each material. However, the same behavior is not seen in the correlation results.

The correlations' standard deviations are higher than those of Case 1 but similar to the results using the experimental data with PVC piping (Case 2). The absolute standard deviations of the data with carbon steel piping are small. However, these values may be inaccurate due to the low number of data points (Table 6).

Table 6 Deviations between the experimental results and those of the correlations under study for Case 3.

Correlation	σ_E	σ_E^2	ϵ_1	ϵ_2	ϵ_3/(%)
Owen [25]	0.050911	0.002592	0.196572	0.412561	90.80
Oliemans et al. [3]	0.138854	0.019280	0.062113	0.210979	69.17
Ishii and Mishima [4]	0.149130	0.022240	0.207599	0.366268	127.23
Pan and Hanratty [16]	0.257598	0.066357	0.142914	0.332758	84.43
Pan and Hanratty [27]	0.212326	0.045083	0.142937	0.342290	81.37
Sawant et al. [9]	0.266142	0.070831	0.122539	0.315803	81.22
Sawant et al. [10]	0.20728	0.042967	0.126856	0.319047	76.59
Karami et al. [28]	0.257747	0.066434	0.142900	0.332654	84.41

4. Conclusions

The entrainment of droplets in gas-liquid annular flows is complex and challenging to model. The correlations available in the literature have arisen from empirical tests or simulations, in which obtaining the entrainment fraction of droplets values is laborious and imprecise. Thus, each correlation deviates to some degree from its experimental situation.

Vertical annular flow with a liquid film lining the interior of the pipe of uniform thickness is the main scenario used for developing correlations in the literature as this removed the need to consider gravitational effects. However, gravity significantly impacts the atomization and deposition of droplets in horizontal pipelines, leading to the over-estimation of the entrainment fraction by these correlations. Also, horizontal flow in most operating conditions does not show a uniform film thickness [28]. Our analysis has made it possible to verify that the entrainment fraction of droplets increases with increasing gas velocity. However, more information is needed to ascertain the influence of the gas-liquid velocity ratio, which influences the interfacial shear, as well as other parameters. There is also a lack of experimental databases assembled under more comprehensive operating conditions and more general correlations. Computational Fluid Dynamics (CFD) tools can help significantly in this respect, as they allow a wide variation in influence parameters, and the results of such numerical studies can generate a better understanding of these and other phenomena related to multiphase flows [41-43].

The variation of some parameters, such as fluid velocity, pipe diameter, and the type of working fluids, results in incorrect results. Although there is a margin of precision, none of the correlations analyzed in this work performs satisfactorily compared to the experimental values used. However, it has been observed that the MacGillivray [33] data for the entrainment fraction of droplets may be imprecise due to the methodology used for its determination. Therefore, each correlation must be cautiously applied due to the conditions and limitations in which they were developed, for a better estimate of the entrainment of droplets, among other parameters.

In conclusion, more in-depth studies are necessary to understand the mechanisms that govern the phenomenon and determine how to develop correlations that both satisfactorily estimate the entrainment of droplets and are applicable in a range of operating conditions and situations of interest.

Acknowledgments

The authors thank the Federal University of Technology — Paraná.

Author Contributions

Mariana P. Koss: literature review, computational code development, production and discussion of results, and article writing; Luiz E. M. Lima: study design, theoretical conceptualization, discussion of results, and article writing and review.

Funding

This study was financed (in part) by the Fundação Araucária — Brasil (Announcement UTFPR/PROPPG 02/2020).

Competing Interests

The authors have declared that no competing interests exist.

References

1. Hewitt G, Hall Taylor NS. Annular two-phase flow. 1st ed. New York: Pergamon Press; 1970.
2. Wallis GB. One-dimensional two-phase flow. New York: McGraw-Hill Book Company; 1969.
3. Oliemans RVA, Pots BFM, Trompé N. Modelling of annular dispersed two-phase flow in vertical pipes. Int J Multiph Flow. 1986; 12: 711-732.
4. Ishii M, Mishima K. Droplet entrainment correlation in annular two-phase flow. Int J Heat Mass Transf. 1989; 32: 1835-1846.
5. Pedras MHJ. Atrito interfacial em escoamento anular transicional/ Marcos Heinzelmann Junqueira Pedras [Internet]. Campinas: University of Campinas; 1993 [cited date 2021 October 15]. Available from: https://hdl.handle.net/20.500.12733/1580362.
6. Alamu MB, Azzopardi BJ. Wave and drop periodicity in transient annular flow. Nucl Eng Des. 2011; 241: 5079-5092.
7. Paleev II, Filippovich BS. Phenomena of liquid transfer in two-phase dispersed annular flow. Int J Heat Mass Transf. 1966; 9: 1089-1093.
8. Azzopardi BJ, Zaidi SH. Determination of entrained fraction in vertical annular gas/liquid flow. J Fluids Eng. 2000; 122: 146-150.
9. Sawant P, Ishii M, Mori M. Droplet entrainment correlation in vertical upward co-current annular two-phase flow. Nucl Eng Des. 2008; 238: 1342-1352.
10. Sawant P, Ishii M, Mori M. Prediction of amount of entrained droplets in vertical annular two-phase flow. Int J Heat Fluid Flow. 2009; 30: 715-728.
11. Al Sarkhi A, Sarica C. Modeling of the droplet entrainment fraction in adiabatic gas-liquid annular flow. Multiph Sci Technol. 2013; 25: 1-23.
12. Dasgupta A, Chandraker DK, Vishnoi AK, Vijayan PK. A new methodology for estimation of initial entrainment fraction in annular flow for improved dryout prediction. Ann Nucl Energy. 2015; 75: 323-330.

13. Bhagwat SM, Ghajar AJ. Modified liquid entrainment fraction correlation for varying pipe orientation and system pressure. Int J Multiph Flow. 2015; 74: 1-4.
14. Cioncolini A, Thome JR. Entrained liquid fraction prediction in adiabatic and evaporating annular two-phase flow. Nucl Eng Des. 2012; 243: 200-213.
15. Lee J, Skorek T, Junk M, Schöffel PJ. Improved correlation of liquid entrainment fraction in horizontal pipes. Nucl Eng Des. 2022; 388: 111615.
16. Pan L, Hanratty TJ. Correlation of entrainment for annular flow in horizontal pipes. Int J Multiph Flow. 2002; 28: 385-408.
17. Colombo LPM, Carraretto IM, Di Lullo AG, Passucci C, Allegrucci A. Experimental study of aqueous foam generation and transport in a horizontal pipe for deliquification purposes. Exp Therm Fluid Sci. 2018; 98: 369-380.
18. Haaland SE. Simple and explicit formulas for the friction factor in turbulent pipe flow. J Fluids Eng. 1983; 105: 89-90.
19. de Paula Jr CF, Lima LEM. Comparison analysis of correlations for interfacial friction factor applied in gas-liquid annular flow in vertical pipes. Rev de Eng Térm. 2017; 16: 54-61.
20. Azzopardi BJ. Drop sizes in annular two-phase flow. Exp Fluids. 1985; 3: 53-59.
21. Swithenbank J, Beer J, Taylor DS, Abbot D, McCreath G. A laser diagnostic technique for the measurement of droplet and particle size distribution. Proceedings of the 14th Aerospace Sciences Meeting; 1976 January 26-28; Washington, D.C., United States. Washington: American Institute of Aeronautics and Astronautics (AIAA).
22. Azzopardi BJ, Govan AH. The modelling of venturi scrubbers. Filtr Sep. 1984; 23: 196-200.
23. Wang G, Zhu Q, Ishii M, Buchanan Jr JR. Four-sensor droplet capable conductivity probe for measurement of churn-turbulent to annular transition flow. Int J Heat Mass Transf. 2020; 157: 119949.
24. Aliyu AM, Almabrok AA, Baba YD, Archibong AE, Lao L, Yeung H, et al. Prediction of entrained droplet fraction in co-current annular gas-liquid flow in vertical pipes. Exp Therm Fluid Sci. 2017; 85: 287-304.
25. Owen DG. An experimental and theoretical analysis of equilibrium annular flows. Birmingham: Faculty of Science and Engineering, University of Birmingham; 1986.
26. Zhang Z, Wang Z, Liu H, Gao Y, Li H, Sun B. Experimental study on entrained droplets in vertical two-phase churn and annular flows. Int J Heat Mass Transf. 2019; 138: 1346-1358.
27. Pan L, Hanratty TJ. Correlation of entrainment for annular flow in vertical pipes. Int J Multiph Flow. 2002; 28: 363-384.
28. Karami H, Pereyra E, Torres CF, Sarica C. Droplet entrainment analysis of three-phase low liquid loading flow. Int J Multiph Flow. 2017; 89: 45-56.
29. Ishii M, Mishima K. Correlation for liquid entrainment in annular two-phase flow of viscous fluid. Final report. Argone, IL: Argonne National Laboratory (ANL); 1981; ANL/RAS/LWR-81-2.
30. Subbotin VI, Deev VI, Pridantsev AI, Andreev VK, Arkhipov VV, Novikov VN, et al. Heat transfer and hydrodynamics in cooling channels of superconducting devices. Cryogenics. 1985; 25: 261-265.
31. Whalley PB, Hewitt GF. The correlation of liquid entrainment fraction and entrainment rate in annular two-phase flow. Final report. Harwell: Atomic Energy Research Establishment (AERE); 1978; AERE-R 9187.

32. Andritsos N, Hanratty TJ. Influence of interfacial waves in stratified gas-liquid flows. AIChE J. 1987; 33: 444-454.
33. MacGillivray RM. Gravity and gas density effects on annular flow average film thickness and frictional pressure drop [Internet]. Saskatoon: University of Saskatchewan; 2004 [cited date 2021 October 15]. Available from: http://hdl.handle.net/10388/etd-09222004-160524.
34. Kesana NR, Skartlien R, Langsholt M, Ibarra R, Tutkun M. Droplet flux measurements in two-phase, low liquid loading, horizontal pipe flow using a high-density gas. J Nat Gas Sci Eng. 2018; 56: 472-485.
35. Python Software Foundation. Welcome to Python.org [Internet]. Python Software Foundation; 2021 [cited date 2021 October 15]. Available from: https://www.python.org.
36. Rossum G. Python development team. Python tutorial. 12th Media Serv; 2018 [cited date 2021 October 15]. Available from: https://docs.python.org/3/tutorial/index.html.
37. Reback J, Jbrockmendel, McKinney W, Van den Bossche J, Augspurger T, Cloud P, et al. Pandas-dev/pandas: Pandas 1.4.2. Zenodo; 2022. doi: 10.5281/zenodo.3509134.
38. The Numpy Community. NumPy v1.21 manual [Internet]. The Numpy Community; 2021 [cited date 2021 October 15]. Available from: https://numpy.org/doc/stable/.
39. Pedregosa F, Varoquaux G, Gramfort A, Michel V, Thirion B, Grisel O, et al. Scikit-learn: Machine learning in Python. J Mach Learn Res. 2011; 12: 2825-2830.
40. Plotly Team. Plotly: The front end for ML and data science models [Internet]. Plotly Team; 2021 [cited date 2021 October 15]. Available from: https://plotly.com.
41. Khan I, Wang M, Zhang Y, Tian W, Su G, Qiu S. Two-phase bubbly flow simulation using CFD method: A review of models for interfacial forces. Prog Nucl Energy. 2020; 125: 103360.
42. Khan I, Wang M, Abdul Basit M, Tian W, Su G, Qiu S. CFD modeling of liquid entrainment through vertical T-junction of fourth stage automatic depressurization system (ADS-4). Ann Nucl Energy. 2021; 159: 108317.
43. Khan I, Wang M, Zhang Y, Tian W, Su G, Qiu S. CFD study on onset of liquid entrainment through ADS-4 branch line in AP1000. Nucl Eng Des. 2021; 380: 111299.